Pergamon

Int. J. Heat Mass Transfer. Vol. 37, No. 7, pp. 1073–1080, 1994

0017-9310/94 $6.00 + 0.00

0017-9310(93)E0024-B

Analysis of CHF location sensibility following heat flux and mass flux variations

G. P. CELATA, M. CUMO and T. SETARO
ENEA, Rome, Italy

(*Received for publication* 18 *November* 1993)

Abstract—An experimental investigation has been performed on critical heat flux (CHF) in subcooled upflow boiling with a uniformly heated vertical tube, using R12 as a coolant, to evaluate the dependence of the CHF location on the variation of the thermal hydraulic parameters affecting the thermal crisis, such as mass flux and heat flux. The test section consists of a stainless steel tube, 7.57 mm i.d., 2.1 m long, uniformly heated using d.c. current. The research showed a different behaviour of the CHF location following mass flux and heat flux variations in the low and in the high quality regions. The sensibility of the CHF location upon the variation of a thermal hydraulic parameter, such as mass flux or heat flux, decreases as the critical quality decreases, and with increasing of the mass flux. At very low critical qualities the CHF location shows a relative insensibility upon large variations of thermal hydraulic parameters. A weak influence of pressure has also been detected.

INTRODUCTION

MANY EXPERIMENTAL studies have been performed on critical heat flux (CHF) of forced convective boiling in uniformly heated vertical tubes fed with subcooled liquid, such as water or refrigerant, to clarify the fundamental nature of CHF in connection with their application in steam generators, in conventional steam boilers and also in nuclear reactors. In 1976 and 1986 Soviet [1] and Canadian authors [2] collected CHF data of uniformly heated round tubes for vertical water upflow and deduced discrete CHF values for the main parameters affecting the CHF, such as pressure, mass flux, and quality. These data have been evaluated and compiled for a fixed tube inner diameter (i.d.) of 8 mm. Starting from the evaluation of the wide amount of experimental data available, the most widely accepted description of the CHF phenomenon is in subdividing the CHF data mainly in two distinctive characters, depending on the critical quality achieved at the thermal crisis. At low quality with subcooled boiling or saturated nucleate boiling, the CHF has strong similarities to pool-boiling critical heat flux, both in mechanism (departure from nucleate boiling) and in behaviour. At high quality, the CHF is associated with convective boiling in annular flow and the mechanism of dryout of the liquid film is verified. Many correlations and models have been developed for low and high quality regions, as reviewed by Marinelli [3], Hewitt [4], Bergles [5, 6], Katto [7] and Whalley [8]. Recently, a new improvement in the research on CHF at very high heat fluxes in the low quality or in subcooled flow boiling region has been demanded by the need of heat removal from components typical of thermonuclear fusion reactors, such as divertors, plasma limiters, neutral beam calorimeters, and ion dump and first-wall armor, as reviewed by Boyd [9, 10] and Celata [11]. However, less attention has been paid to the study of the dependence of CHF location on the variation of a thermal hydraulic parameter such as mass flux or heat flux. Particularly with water, once the CHF is reached, the burnout of the tube occurs at the end of the test section (under steady-state conditions and uniformly heated tubes) and the accuracy of the thermal hydraulic parameter values may be affected by the step of the variation of the parameters near the thermal crisis, for example, if we increase step by step the heat flux during the experiment, the accuracy of the CHF depends on the amplitude of the step variation of heat flux we deliver to the test section. As is well known, the behaviour in the proximity of the CHF point in the low quality region shows a hysteresis effect as the heat flux is increased and then decreased, while this effect is not present in the high quality region (see Whalley [8]). The aim of the present work is to give a contribution in the understanding of the intrinsic uncertainty of experimental data connected to the two different mechanisms of thermal crisis. The report gives the results of an investigation performed with a uniformly heated vertical tube, fed with subcooled R12, to evaluate the influence of a parameter variation on the thermal crisis location with respect to the end of the tube. A comparison of experimental data with current correlations has been reported.

EXPERIMENTAL APPARATUS

The experimental loop, schematically represented in Fig. 1, consists mainly of a piston pump, an electric heater, a condenser and a liquid tank. The maximum operating pressure of the loop is 3.5 MPa, while the maximum specific flow rate is 1800 kg m^{-2} s^{-1}; the available electrical power (d.c.) is 10 kW for the electric heater and 15 kW for the test section. The test section is

NOMENCLATURE

G	mass flux [kg m^{-2} s^{-1}]
Δi	latent heat of vaporization [kJ kg^{-1}]
L	length [m]
p	pressure [MPa]
q''	heat flux [kW m^{-2}]
T	temperature [K]
V	specific volume [m^3 kg^{-1}]
X	quality
z	axial coordinate [m].

Subscripts

CHF	pertains to the critical heat flux condition
ex	experimental value
in	initial, inlet
L	pertains to the liquid phase
sat	pertains to saturation conditions
sub	subcooled
th	theoretical value
V	pertains to the vapour phase
w	wall.

an industrial stainless steel (AISI 316), circular duct uniformly heated (Joule effect) over a length of 2100 mm, with an inner diameter of 7.57 mm and a wall thickness of 0.97 mm. The inner surface of the tube is characterized by a cavity density of about 3.5×10^9 cavities m^{-2}, with a cavity density of 2.2×10^9 cavities m^{-2} for the size below 0.5 μm. The cavity density has been evaluated using a Digital Image Measurement System connected to an electronic microscope. The Digital Image Measurement System evaluates the number of cavities into the inner surface of a tube sample and calculates the equivalent mouth diameter of each cavity. A typical electron micrograph of the inner surface of the test section is shown in Fig. 2: the cavities are the black spots and the scale is 1 cm = 0.5 μm. Test section instrumentation consists of 0.5 mm, K-Type insulated thermocouples distributed according to the scheme of Fig. 3 for the wall (two) and the fluid (seven) temperature measurements. Two pressure transducers measure the pressure at the inlet and outlet of the test section. A turbine flow meter measures the volumetric flow rate at the inlet of the test section. The heating power has been gaged with a watt meter. Instruments accuracy is listed in Table 1. The fluid flow is upwards, with subcooled inlet conditions. Before introducing the R12 in the experimental loop, vacuum up to 0.1 Pa has been obtained using a vacuum pump. After the fluid is introduced, the pressure inside the loop always exceeds the atmospheric pressure, not allowing any air re-entrance. Data acquisition is accomplished by a MacIntosh Computer.

PHYSICAL PROPERTIES EVALUATION

Regarding the analysis of the data and the comparison with predictive methods, all thermodynamics properties, such as density, enthalpy and saturation temperature, for R12 were calculated by the Carnahan–Starling–DeSantis (CSD) equation of state, as proposed by Morrison and McLinden [12]. The ability of the CSD equation of state in predicting the p–v–t behaviour of R12 is shown in Table 2, where the RMS errors of the equation of state in representing the ASHRAE data [13] of saturation pressure, saturated liquid and vapour volume and vaporization enthalpy of the fluid are listed.

EXPERIMENTAL RESULTS AND DATA ANALYSIS

The ranges of variation of the parameters in the tests performed were from the combination of the following values:

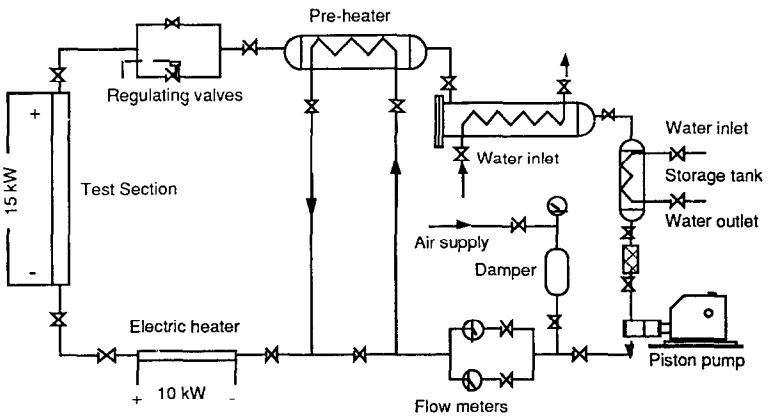

FIG. 1. Schematic of the experimental loop.

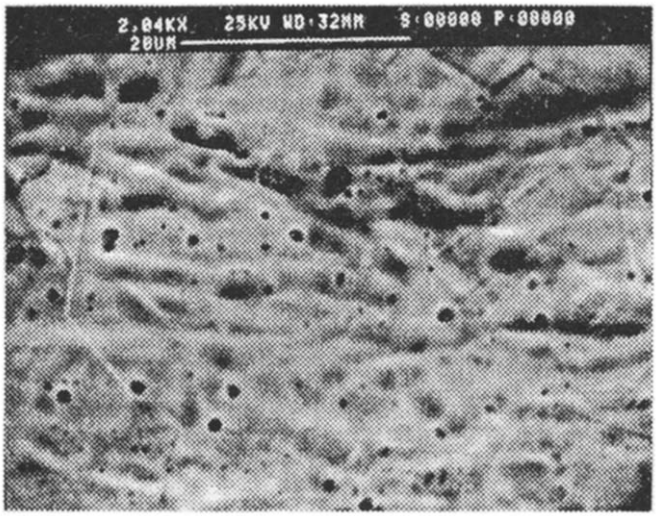

FIG. 2. Electron micrograph of the inner surface of the test section: scale 1 cm: 0.5 μm.

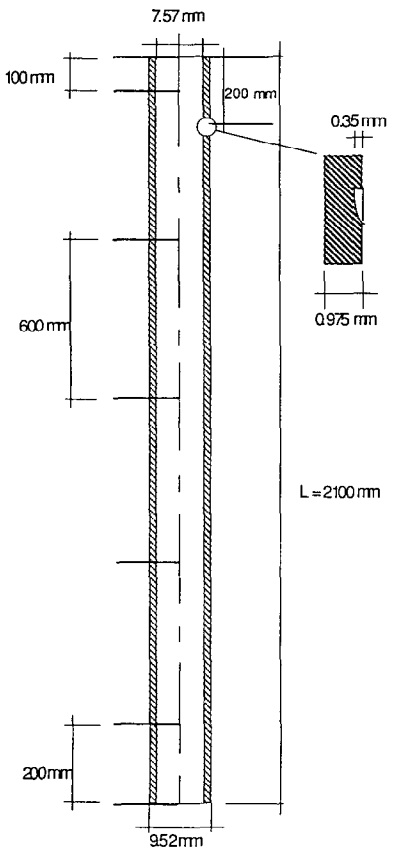

FIG. 3. Schematic of the test section.

Table 1. Instruments and their accuracy

Parameter	Instrument	Accuracy
Heating power	Wattmeter	±0.3 W
Flow rate	Turbine flow meter	±0.15 $dm^3 h^{-1}$
Temperature	K-Type tc insulated	±0.1 K
Pressure	Sealed strain-gauge	±4 kPa

Test matrix

Fluid	R12 (CCl_2F_2)
q'' [kW m^{-2}]	20–70
p [MPa]	1.2–2.5
G [kg $m^{-2} s^{-1}$]	400–1600
$\Delta T_{sub,in}$ [K]	2

The thermal crisis is verified by the sudden increase of the measured wall temperature at the monitored location, as shown in Fig. 4. The tests were performed to evaluate the relationship between the variation of mass flux and heat flux and the variation of the thermal crisis location. The test procedure consists first in reaching the CHF condition at the end of the test section ($z = 2.1$ m) for fixed mass flux, inlet subcooling and pressure, then in applying small variations of the parameter step by step (increase of the heat flux or decrease of the mass flow rate). After each variation the restoration of steady-state conditions is awaited, and the occurrence of thermal crisis at location $z = 1.9$ m is checked. In all the tests the variation in the thermal crisis location is equal to $\Delta z = 0.2$ m. In the case of mass flux variations the flow rate at the inlet of the test section is decreased, while for the heat flux variations the heating power supplied to the test section is increased. The experimental results have been reported in terms of the absolute value of the ratio between the quota variation and the mass flux or the heat flux variation, $\Delta z/\Delta G$ and $\Delta z/\Delta q''$, respectively. The effect of the mass flux variation on the crisis location, in terms of $\Delta z/\Delta G$, vs

Table 2. RMS of CSD equation of state referred to ASHRAE values of saturation pressure, saturated liquid and vapour volume and vaporization enthalpy for R12 [12]

	RMS (%)			
Refrigerant	p_{sat}	V_L	V_V	Δi
R12	0.26	0.05	0.29	0.74

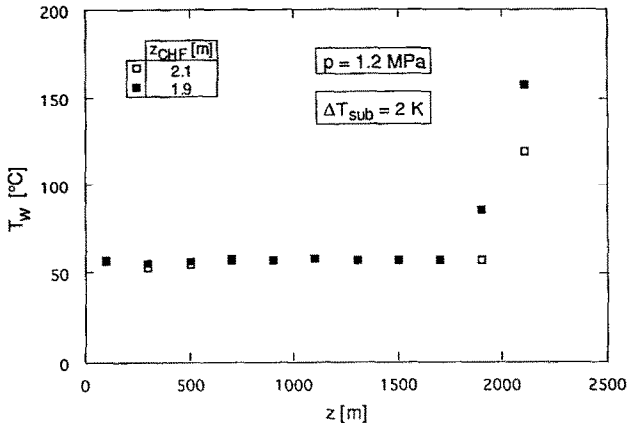

FIG. 4. Typical wall temperature profiles at the beginning and at the end of mass flux variation test.

the mass flux at the initial condition of the test ($z = 2.1$ m) has been plotted in Fig. 5, using the pressure as a parameter. Looking at the figure, the dependence of the thermal crisis location on a mass flux variation decreases as the initial mass flux increases. However, above 1000 kg m^{-2} s^{-1}, the influence of mass flux variations on thermal crisis location becomes small and slightly affected by the initial value of the mass flux. The system pressure weakly affects the dependence of crisis location on mass flux variations, tending to increase the influence of the variation on the crisis location as the pressure increases. The effect of the heat flux variation on the thermal crisis location, expressed as the absolute value of the ratio $\Delta z/\Delta q''$, has been plotted in Fig. 6 vs the mass flux at the initial condition of the test ($z = 2.1$ m), using the pressure as a parameter. In the figure, the influence of the heat flux variation on the thermal crisis location tends to decrease as the mass flux increases and to increase with the pressure increasing.

An interpretation of the different trend of experimental results at lower and higher mass fluxes and pressures may be given examining the thermal hydraulic conditions and the connected mechanism of crisis. As is well known from previous investigations [14, 15], and particularly that carried out on burnout by Levitan and Lantsman [15], there are mainly two different mechanisms of thermal crisis: the departure from nucleate boiling (DNB) and the dryout. The first mechanism is associated with the nucleate boiling heat transfer regime and is typical of low quality and high heat flux conditions, being characterized by a variation of the critical quality with the CHF. The CHF in the low quality region shows a hysteresis effect as the heat flux is increased and then decreased, with strong simulations to pool-boiling critical heat flux. This would suggest the variation of the CHF location due to heat flux and mass flux variations to be of less significance. An experimental verification of the presence of the hysteresis effect in the boiling curve at the CHF is reported in Fig. 7(a), for a typical R12 DNB-type CHF. The dryout, as verified by Levitan

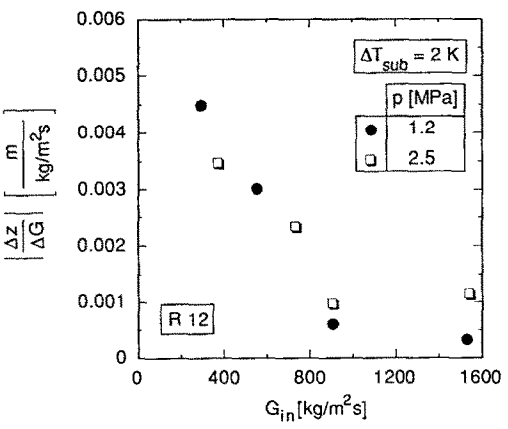

FIG. 5. Effect of the mass flux variation $\Delta z/\Delta G$, vs the mass flux at the initial condition of the test ($z = 2.1$ m), with the pressure as a parameter.

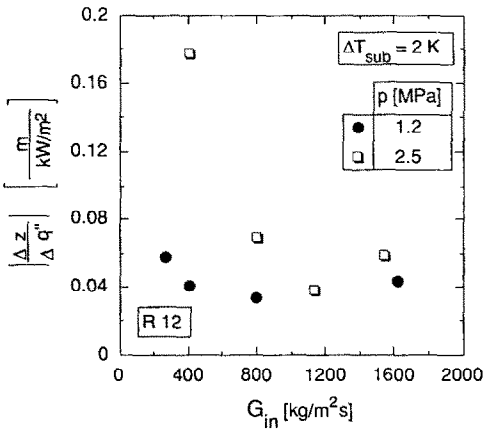

FIG. 6. Effect of the heat flux variation, $\Delta z/\Delta q''$, vs the mass flux at the initial condition of the test ($z = 2.1$ m), with the pressure as a parameter.

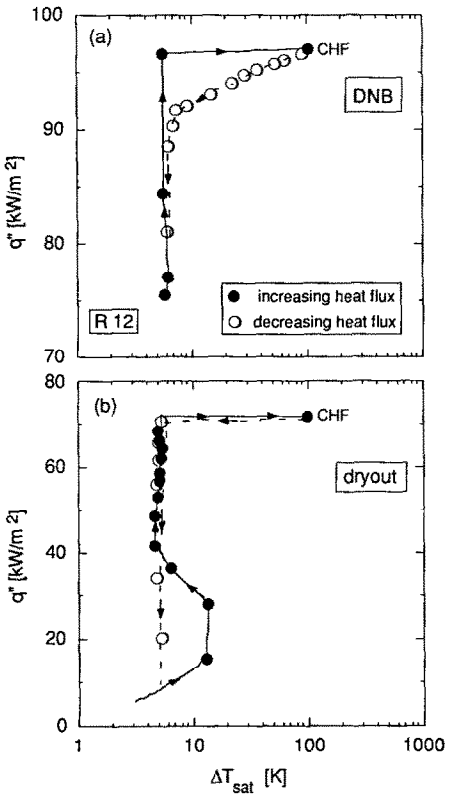

FIG. 7. R12 experimental boiling curves for DNB (a) and dryout-type (b) CHF.

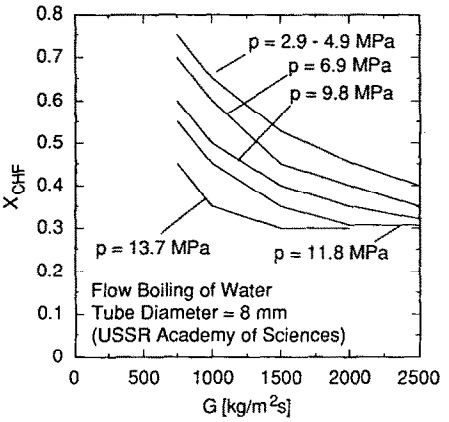

FIG. 8. Dryout curves for water at different pressures (USSR Academy of Sciences [1, 15]).

and Lantsman [15], is associated with the convective boiling regime and is typical of higher qualities and lower heat fluxes, with a limiting value of critical quality essentially independent of the heat flux. No hysteresis effect on the CHF is present in the high quality region, as shown in the dryout experiment plotted in Fig. 7(b). In contrast with the presence of the hysteresis, associated with the DNB-type mechanism of the CHF, the absence of the hysteresis phenomenon would suggest the location of the CHF to be very sensitive to variations of the thermal hydraulic parameters. Levitan and Lantsman [15] recommended the values of the limiting dryout quality conditions for low heat fluxes, with water as a coolant, and presented graphically their results for a 8 mm i.d. tube, as shown in Fig. 8. The burnout data have also been tabulated by the members of the USSR Academy of Sciences [1]. The plot in Fig. 8 clearly indicates that increasing the mass flux the dryout quality decreases. At a lower value of the critical quality, with respect to the dryout curve, the boiling crisis may be thought to be of the DNB type. Starting from the above premises and using the scaling laws proposed by Ahmad [16] to deduce the dryout curves for the refrigerants, it is possible to compare present experimental data with the derived dryout curves, as shown in Fig. 9. In the figure, the critical quality at the thermal crisis location has been plotted vs the mass flux together with the corresponding dryout curve, scaled for the fluid and the geometry used in the present tests. The left-hand side graphs show tests with a mass flux variation (tests 1–8) and the graphs on the right show the data of the heat flux variation (tests 9–16). In all the graphs, the empty and closed symbols represent the initial and the final condition of each test, respectively, and the number near each symbol in the graphs refers to each single run. In the top left-hand side graph, where the data at the lower pressure are plotted, the first two tests (1 and 2) are characterized by the convective boiling regime with a dryout mechanism of thermal crisis at both the examined locations (2.1 and 1.9 m). The variation of mass flux connected with the fixed variation of thermal crisis location ($\Delta z = 0.2$ m) is small and, thus, the sensibility to mass flux changes in the dryout region at high quality is large, as previously noticed in Fig. 5. The mass flux effect on the CHF at the dryout conditions in annular flow is already known, as reported by Hewitt and Hall-Taylor [17]. The authors state that for given channel geometry and inlet subcooling, the dryout heat flux increases rapidly as the mass flux increases at low mass velocities, and more slowly at high mass flux. Consequently, for a given CHF condition the sensibility to a mass flux variation of the crisis location reduces rapidly with increasing mass flux in the low mass flux–high quality region and more slowly at the high mass flux–low quality region. Nevertheless, there is an almost linear relationship between sensibility of thermal crisis location to the mass flux variation and the length of channel in annular low, since the sensibility increases with increasing of the annular flow region extension in the channel.

Considering the other two tests at high mass flux (3 and 4) plotted in the top left-hand side graph of Fig. 9, the initial CHF condition (2.1 m) is associated with DNB mechanism of thermal crisis and with the intermediate–low quality region while, at the end of the variation, the thermal crisis at the lower location (1.9 m) is to be associated with the dryout mechanism,

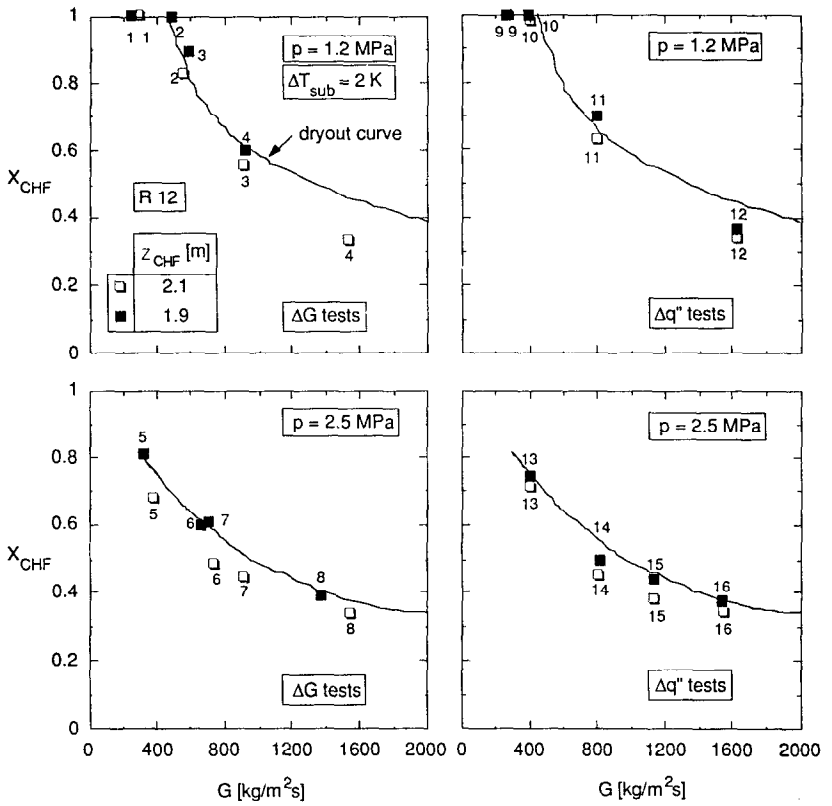

FIG. 9. Comparison of experimental data with the derived dryout curves.

lying the data point on the dryout curve. This trend is also verified in the other tests of mass flux variation at higher pressure (tests 5–8), as shown in the bottom left-hand side graph and in most of the heat flux variation data, plotted in the right-hand side graphs of Fig. 9. Finally, two of the tests performed varying the heat flux (test 12 at 1.2 MPa and tests 14 and 15 at 2.5 MPa) show a DNB mechanism of thermal crisis associated to both the initial and final location of thermal crisis. Those tests have also shown a lower sensibility of the CHF quota to the heat flux variation, as seen in Fig. 6, confirming the hypothesis that in the low quality region, where the nucleate boiling regime is present and the DNB mechanism of thermal crisis is dominant, the influence of a global thermal hydraulic parameter variation is weaker than in the high quality region, because of the presence of a hysteresis effect on the CHF. In conclusion, in the annular flow, high quality region, where a dryout-type mechanism of the thermal crisis is expected, small variations of one thermal hydraulic parameter greatly affect the location of the thermal crisis. In the low quality region, corresponding to churn and semi-annular flow, high mass flux, nucleate boiling heat transfer regime and DNB-type mechanism of the thermal crisis, there is a weak influence of a variation in the thermal hydraulic parameters. Finally, in the intermediate cases where the initial condition is a thermal crisis of DNB-type and the final condition is a dryout-type CHF, the sensibility of the CHF location due to variations of thermal hydraulic parameters decreases as much as the initial critical quality is low and far from the corresponding dryout quality. From the above evaluations, it follows that dryout tests have to be performed with the highest possible precision, since even a little uncertainty in the thermal hydraulic parameters (e.g. oscillations of the mass flow rate, etc.) as well as in the measurement system may play an important role in the determination of the physical phenomenon. Nevertheless, also in the test of DNB data a good precision is desirable, even if a larger uncertainty may be allowed.

EXPERIMENTAL DATA PREDICTION

A wide number of correlations and models developed to predict the CHF in steady-state forced convective boiling inside tubes are available in literature. Among the correlations developed for water and Refrigerants the most widely used are the modified CISE correlation [18] and the Katto correlation [19]. Those two correlations, based on a physical analysis of the thermal crisis phenomena in both low and high quality region, have been tested on 107 data of R12 CHF in vertical upflow steady-state conditions, part of a wider CHF data bank available at ENEA (for

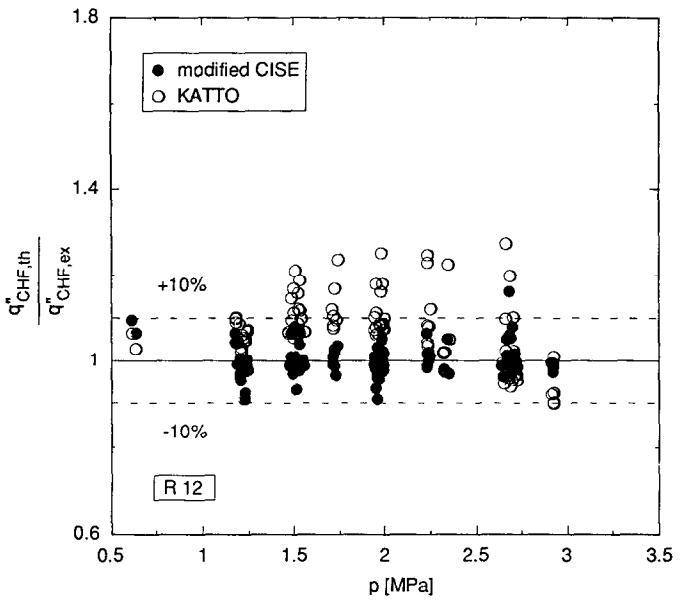

FIG. 10. Comparison of the predicted CHF by modified CISE [18] and Katto [19] correlations with the experimental data [20].

further detail see the paper by Celata *et al.* [20]), as reported in Fig. 10. In applying the two above correlations, the inlet conditions have been used. The results plotted in the figure, in terms of theoretical-to-experimental CHF ratio, show a good performance of the modified CISE correlation, within a $\pm 10\%$ error band, while a larger scattering is obtained in the case of the Katto correlation and a tendency to overpredict the experimental CHF at pressure below 2.0 MPa.

Concerning the ability of predicting the effect of a parameter variation on the thermal crisis location, the absolute value of the fixed quota variation ($\Delta z = 0.2$ m) and mass flux ratio, $\Delta z/\Delta G$ vs the initial mass flux has been plotted in Fig. 11, using the pressure as a parameter. In the figure, the lines refer to the correlation predictions and the points refer to the experimental data. The modified CISE correlation (top graph) shows a better performance than the Katto correlation (bottom graph) at low mass flux-high quality region while the Katto correlation tends to become equivalent to the modified CISE correlation at intermediate-high mass fluxes. As far as heat flux variations are concerned, the performances of the two above correlations in predicting experimental data are plotted in Fig. 12, using the pressure as a parameter. The two correlations give similar (good) predictions of the CHF location sensibility. In conclusion, both the correlations well predict the variation of thermal crisis location due to the examined thermal hydraulic parameters variations.

CONCLUSIONS

The analysis of the experimental data on CHF in steady-state upflow forced boiling of R12 shows a decreasing sensibility of the thermal crisis location following a thermal hydraulic parameter variation (such as mass flux or heat flux variation) with the increasing of initial mass flux. An explanation of the trend of experimental results may be given examining the thermal hydraulic conditions and the connected mechanism of crisis at the beginning and at the end of the parameters variation. In the low quality region, where the nucleate boiling regime is present together with a consistent hysteresis effect, and the DNB mechanism of thermal crisis is dominant, the influence of a thermal hydraulic parameter variation is weaker than in the high quality region, where the convective boiling and the dryout mechanism of thermal crisis are present without any hysteresis effects. In those cases where the DNB-type mechanism of the CHF is present at the beginning of the variation and the dryout-type mechanism appears at the end of the variation, the influence of the thermal hydraulic parameter variation decreases as much as the inital critical quality is low and far from the corresponding dryout quality.

The comparison of the thermal crisis location variation with mass flux and heat flux variations, obtained using the modified CISE and the Katto correlations, with the experimental data shows a good performance of the modified CISE for all the mass fluxes tested, while the Katto correlation seems to be less accurate at low mass fluxes, being globally able to follow the experimental data trend.

Acknowledgements—The authors are deeply indebted to Mr G. Farina, who performed the experimental runs. Thanks are also due to Mrs A. M. Moroni for the editing of the article.

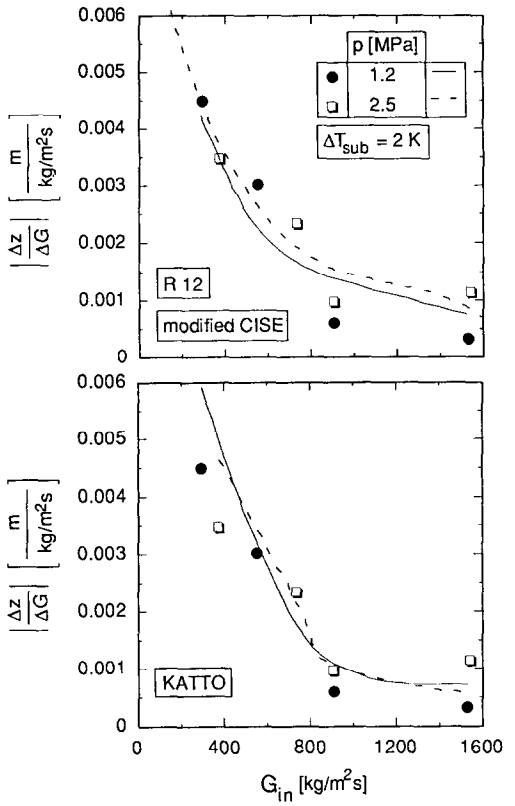

FIG. 11. Comparison between experimental and calculated CHF location sensibility for mass flux variations, using modified CISE [18] and Katto [19] correlations.

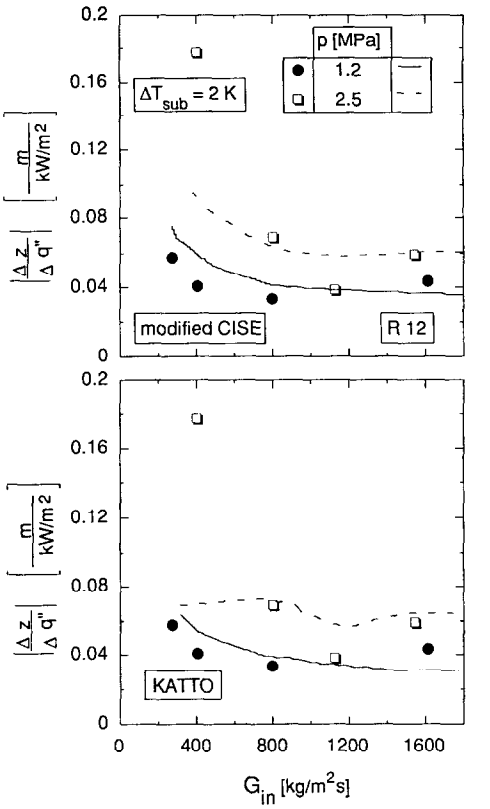

FIG. 12. Comparison between experimental and calculated CHF location sensibility for heat flux variations, using modified CISE [18] and Katto [19] correlations.

REFERENCES

1. USSR Academy of Sciences, Tabular data for calculating burnout when boiling water in uniformly heated round tubes, *Teploenergetika* **23**, 90–92 (1976).
2. D. C. Groeneveld, S. C. Cheng and T. Doan, The CHF look-up table, a simple and accurate method for predicting critical heat flux, *Heat Transfer Engng* **7**, 46–62 (1986).
3. V. Marinelli, Critical heat flux: a review of recent publications, *Nuclear Technol.* **34**, 135–171 (1977).
4. G. F. Hewitt, Critical heat flux in flow boiling, *Proc. 6th Int. Heat Transfer Conference Toronto*, Vol. 6, pp. 143–171 (1978).
5. A. E. Bergles, Burnout in boiling heat transfer, Part I: Pool boiling systems, *Nuclear Safety* **16**, 29–42 (1975).
6. A. E. Bergles, Burnout in boiling heat transfer, Part II: Subcooled and low quality forced-convective systems, *Nuclear Safety* **18**, 154–167 (1977).
7. Y. Katto, Critical heat flux in boiling, *Proc. 8th Int. Heat Transfer Conference, San Francisco*, Vol. 1, pp. 171–180 (1986).
8. P. B. Whalley, *Boiling Condensation and Gas–Liquid Flow*, pp. 155–166. Oxford University Press, Oxford (1987).
9. R. D. Boyd, Subcooled flow boiling critical heat flux (CHF) and its application to fusion energy components. Part I: A review of fundamentals of CHF and related data base, *Fusion Technol.* **7**, 7–30 (1985).
10. R. D. Boyd, Subcooled flow boiling critical heat flux (CHF) and its application to fusion energy components. Part II: A review of microconvective, experimental, and correlational aspects, *Fusion Technol.* **7**, 31–52 (1985).
11. G. P. Celata, A review of recent experiments and prediction aspects of burnout at very high heat fluxes, *Proc. International Conference on Multiphase Flows '91, Tsukuba, Tsukuba*, Vol. 1, pp. 31–40 (1991).
12. G. Morrison and M. McLinden, Application of a hard sphere equation of state to refrigerants and refrigerant mixtures, NBS Technical Note 1226, NBS, Gaithersburg, Maryland (1986).
13. American Society of Heating, Refrigerant and Air Conditioning Engineer, Inc., ASHRAE Handbook of Fundamentals, New York (1981).
14. J. G. Collier, *Convective Boiling and Condensation—Second Edition*, pp. 248–274. McGraw Hill, New York (1981).
15. L. L. Levitan and F. P. Lantsman, Investigating burnout with flow of steam–water mixture in a round tube, *Teploenergetika* **22**, 80–83 (1975).
16. S. Y. Ahmad, Fluid to fluid modelling of critical heat flux: A compensated distortion model, *Int. J. Heat Mass Transfer* **16**, 641–661 (1973).
17. G. F. Hewitt and N. S. Hall-Taylor, *Annular Two-Phase Flow*, pp. 219–252. Pergamon Press, Oxford (1970).
18. S. Bertoletti, G. P. Gaspari, C. Lombardi, G. Peterlongo, M. Silvestri and F. A. Tacconi, Heat transfer crisis with steam–water mixtures, *Energia Nucleare* **12**, 121–170 (1965).
19. Y. Katto and H. Ohno, An improved version of the generalized correlation of critical heat flux for the forced convective boiling in uniformly heated vertical tubes, *Int. J. Heat Mass Transfer* **27**, 1641–1648 (1984).
20. G. P. Celata, M. Cumo, F. D'Annibale and G. E. Farello, Critical heat flux in transient flow boiling during simultaneous variations in flow rate and thermal power, *Experimental Thermal and Fluid Science* **2**, 134–145 (1989).